Electrochemical Performance of Nano-SiC Prepared in Thermal Plasma

Ch. Venkateswara Rao[1], S.K. Singh[2] and B.Viswanathan[1]

[1]National Centre for Catalysis Research, Department of Chemistry, Indian Institute of Technology, Madras Chennai - 600 036

[2] Institute of Minerals & Materials Technology (formerly Regional Research Laboratory), Bhubaneswar - 751 013

Abstract

The possibility of using SiC as support for Pt and employing them as alternate electrodes for fuel cell applications has been examined. The prepared SiC has been characterized by a variety of analytical methods and shown to possess better surface characteristics compared to carbon.

Key words: SiC support; fuel cell electrode; nanoSiC; thermal plasma

1. Introduction

Some of the important requisites of support materials for electrochemical device applications are good electrical conductivity, chemical and structural stability under operating conditions i.e., operating temperature, partial pressure and flow rate of reactants [1]. At present, carbon is the commercially exploited support material for electrode applications. But the weak oxidation resistance of carbon as support hinders its use for high-temperature oxidative reactions. Typically, CO_2 formation is generalized according to the equation: $C + 2H_2O \rightarrow CO_2 + 4H^+ + 4e^-$; $E^\circ = + 0.207$ vs NHE [2]. Corrosion of the carbon support accelerate under acidic environment (pH <1), high water content, high temperature (50-90 ˚C), high potential (0.6-1.2 V vs NHE) and high oxygen concentration [3-5]. Platinum supported on carbon black is widely used as fuel cell electrocatalyst [6]. Under the operating conditions of fuel cell, carbon corrosion causes the agglomeration of Pt particles and results in the deterioration of fuel cell. Moreover, Pt catalysts accelerate the rate of carbon corrosion to CO_2, which may cause permanent carbon loss, a loss of catalyst activity, and, in the extreme, a structural collapse of the electrode [7-9]. As a result, carbon support will not be good enough for longer duration in

terms of activity. It is consequently of interest to develop new support materials that can efficiently avoid the drawbacks linked to classical carbon supports. Silicon carbide (SiC) exhibits high thermal conductivity, high resistance towards oxidation, high mechanical strength, low specific weight and chemical inertness; all properties required for a good heterogeneous catalyst support material [10,11]. However, preparation of high surface area SiC is a major problem. Obviously, SiC produced by Acheson process is not suitable for this type of applications. Amongst the various methods used for synthesis of ultrafine powders, the plasma processing appears to be most promising [12]. Thermal Plasma with high temperature gas-phase chemistry within the plasma environments provides an attractive route for ultrafine powder synthesis. Plasma synthesis has several important advantages relative to various other powder synthesis techniques. The peak temperature is higher than that in any other method; the energy density is high; and cooling in the flow direction is rapid. Relatively high throughput can be achieved in a small reactor. Post synthesis milling, a major contamination source for conventionally produced powders, is not required because the process inherently produces sub-micron particles.

Therefore, an attempt has been made in this present work to study the electrochemical performance of the SiC supported Pt nanoparticle catalyst. The nano-SiC for this purpose has been prepared from coarse SiC in thermal plasma following a patented process [13].

2. Experimental Section

2.1. Preparation of nano-SiC

Preparation of nano SiC powder was carried out in an indigenously developed in-flight processing thermal plasma reactor operating at atmospheric pressure [13]. The reactor assembly consists of a water cooled stainless steel chamber where the water cooled copper electrodes are arranged in a vertical configuration and both the electrodes are provided with detachable graphite end pieces for striking the arc. The top copper electrode (cathode) has an axial hole through which the plasma forming gas is injected to the plasma chamber. A powder feeder is attached to this electrode for feeding the powder to the plasma zone through the axial hole. Both the top and bottom electrodes are connected to a DC plasma power source.

Commercial grade SiC (100–500 micron) was taken as the precursor material for preparation of nano SiC. The arc was struck between the top and the bottom electrodes and the arc expansion and stabilization was established by the vertical movement of the electrodes. Coarse SiC was then fed to the plasma from the powder feeder along with the argon plasma forming gas. The coarse SiC was evaporated in the plasma to form vapour of silicon carbide which was then deposited on the cold wall of the reactor chamber in the form of nano SiC powder. The reactor and the process are described elsewhere [13]. A typical operating condition is arc current of 350 A and load voltage of 50 V.

2.2. Preparation of SiC supported Pt nanoparticle catalyst

20 wt% Pt/SiC has been prepared by hydrogen reduction method [14]. To the 200 mg of SiC sample, required amount of 5% hexachloroplatinic acid solution ($H_2PtCl_6.xH_2O$) was added and stirred for 2 hr. After that it was filtered and dried in hot air oven at 348 K for 2 hr. Then the resulting material was made into fine powder and reduced under H_2 atmosphere at 723 K for 2 hr. The amount of Pt loaded on SiC was estimated by spectrophotometric method [15]. It was estimated to be 18.4 wt%.

2.3. Physical Characterization

X-ray diffraction (XRD), scanning electron microscopy (SEM) and transmission electron microscopy (TEM) were used to identify the crystal structure, morphology and particle size respectively. The X-ray diffraction (XRD) patterns of the catalysts were obtained with a Philips Powder Diffraction System (Model PW 1830) using a Cu Kα source operated at 30 keV at a scan rate of 0.05^o s^{-1}. Transmission electron microscope (TEM) images were obtained by using a high-resolution JEOL 2010 TEM system operated with a LaB_6 filament at 200 kV. The samples were dispersed in ethanol under ultrasonication and dropped on the carbon-coated grid and then imaged. Scanning electron microscope with EDX (FEI, Model: Quanta 200) was used to observe the surface morphology and composition of the catalysts.

2.4. Electrochemical measurements

ORR measurements were performed at room temperature by cyclic voltammetry using a potentiostat (BAS 100 electrochemical analyzer) connected to a three electrode cell assembled with glassy carbon (GC) disk as the working electrode, Ag/AgCl, 3.5 M KCl (+0.205 V vs. NHE) as the reference and Pt foil as the counter electrodes, respectively. Oxygen saturated 0.5 M H_2SO_4 was the electrolyte. The electrode was fabricated as described by Schmidt et al [16]. Briefly, 4 mg of Pt/SiC catalyst was dispersed in 4 ml of isopropanol by ultrasonication for 15 min. GC disk (0.07 cm^2) was polished to a mirror finish with 0.05 μm alumina suspensions before each experiment and served as an underlying substrate of the working electrode. An aliquot of 20 μl catalyst suspension was pipetted onto the carbon substrate. After evaporation of isopropanol in an argon stream, 10 μl of a diluted Nafion® solution (Aldrich, 5 wt.% in 15-20% water/low aliphatic alcohols) were pipetted on the electrode surface in order to attach the catalyst particles onto the GC disk. After preparation, the electrodes were immersed in deaerated 0.5 M H_2SO_4. Then the linear sweep voltammograms (LSV) were recorded between +0.2 V and +1.2 V vs NHE at a scan rate of 2 mV/s. For the oxygen reduction experiments, the electrolyte was saturated with pure oxygen and recorded the linear sweep voltammograms (LSV) between +0.2 and +1.2 V vs NHE at a scan rate of 2 mV/s. Oxygen reduction activity was calculated by taking the difference in activity at +0.7 V vs NHE in Ar- and O_2- saturated 0.5 M H_2SO_4. Current densities are normalized to the geometric area of the glassy carbon substrate (0.07 cm^2).

3. Results and discussion

3.1. XRD measurements

X-ray diffraction patterns of the SiC, Pt/SiC and commercial Pt/C catalysts are shown in Fig. 1(a)-(c). In the as-synthesized SiC and Pt/SiC samples, the larger diffraction peaks at 2θ values of 35.6°, 41.5°, 59.9° and 71.7° corresponds to the (111), (200), (220) and (311) planes of β-phase of SiC and the smaller diffraction peaks at 2θ values of 33°, 45° and 52.5° corresponds to the (100), (105) and (106) planes of α-phase of SiC (fig. 1(a)&(b)). Pt/SiC and commercial Pt/C samples exhibit five characteristic diffraction peaks at 2θ values around 40°, 46.3°, 67.9°, 81.4° and 86.7° corresponds to the

(111), (200), (220) and (311) planes of face-centered cubic (fcc) structure of Pt (JCPDS card 4-802). The broad diffraction peaks of Pt in the Pt/SiC and Pt/C catalysts are indicative of the nano-sized Pt. The diffraction peak at around 2θ value of 25° corresponds to the (002) diffraction peak of the hexagonal structure of the carbon support. In the case of SiC and Pt/SiC samples, very small amounts of carbon were observed. Since the synthesis of SiC was carried out at high temperature, smaller amounts of the formation of carbon cannot be ruled out.

3.2. SEM and TEM analysis

Fig. 2 represents the scanning electron micrographs of SiC and Pt/SiC. Agglomerates of two dimensional networks of SiC chains can be seen in Fig. 2(a). Similar structure can be seen in the case of Pt/SiC catalyst also (Fig. 2(b)). Transmission electron micrographs of SiC and Pt/SiC give us the clear identification of the two dimensional network nanostructures of SiC chains (Fig. 3(a) & (b)). It can be concluded that the morphology of the SiC was retained even after loading Pt. Well dispersed and spherical shaped Pt nanoparticles with narrow size distribution on the SiC network chains are observed and the average particle size of Pt is calculated to be 3.5 nm. Inset shows the spherical shaped Pt particle embedded in SiC matrix. For comparison, TEM image of commercial Pt/C is also shown in Fig. 3(c). The average particle size of Pt in the case of commercial catalyst is 3.7 nm, which is in good agreement with the literature reports [17,18]. EDX analysis reveals that the synthesized SiC composed of Si, C and a small quantity of oxygen and Pt/SiC is composed of Pt, Si, C and a small quantity of oxygen (Fig. 4).

Since the Pt particles are spherical, specific surface area of Pt (A_{sp}) in an electrode was calculated by using Eq. 1 [19]:

$$A_{sp} = \frac{6000}{\rho d} \quad \ldots\ldots\ldots\ldots\ldots (1)$$

where ρ is the Pt density, d is the particle size (in nm) with A_{sp} given in m^2/g. we assumed bulk density of Pt (21.45 g/cm^3) as density of Pt in the Pt/C catalysts in

calculation. The obtained results are given in Table 1. The results show that the as-synthesized Pt/SiC and commercial Pt/C are having similar electroactive surface area. Within the error limits, these values are in good agreement with the specific surface area calculated from Pt particle size in the investigated Pt catalysts.

3.3. Electrochemical performances

The electrochemical active surface area of the Pt/SiC and Pt/C electrocatalysts is determined from ex-situ cyclic voltammetry analysis. Fig. 5 shows the steady-state cyclic voltammograms (CVs) of Pt/SiC and commercial Pt/C catalysts between -0.05 and +1.2 V vs NHE at a scan rate of 25 mV/sec. During the anodic scan, hydrogen is adsorbed between -0.05 and +0.35 V vs NHE and surface platinum oxides are formed beyond +0.8 V vs NHE. During the cathodic scan, the surface platinum oxides are reduced between +1.0 and +0.5 V vs NHE and hydrogen is desorbed at potentials more cathodic than +0.35 V vs NHE at the both Pt catalysts [20]. The carbon-supported Pt particles possess some degree of low coordinated crystal planes, and hence the hydrogen adsorption/desorption features between +0.4 and +0.0 V vs RHE are different from the bulk polycrystalline Pt. It is an indicative of the preferential orientation of Pt in (111) manner [21]. However, not well-defined hydrogen adsorption/desorption peaks (broad peaks) on the Pt/SiC catalyst was found, suggesting that the high dispersion of the catalysts with the disordered surface structure [22]. These broad peaks are indicative of the orientation of all the planes in equal probability. Hydrogen absorption and hydrogen desorption peaks appeared between +0.0 and +0.4 V in the catalysts have used to calculate the electrochemical active surface area (EAS) by using the Eq. 2 [23].

$$EAS = \frac{Q_H}{0.21L} \; ; \; Q_H = \frac{Q_1 + Q_2}{2} \quad \ldots\ldots\ldots (2)$$

where Q_H was the columbic charge for hydrogen desorption, which was calculated as the mean value between the amounts of charge exchanged during the electro adsorption (Q_1) and desorption (Q_2) of hydrogen on Pt sites. In Eq. (2), EAS is given in cm^2/g; Q_H in mC/cm^2; 0.21 mC/cm^2 is the charge required for oxidation of a single molecule of H_2 on a polycrystalline Pt surface of 1 cm^2 [24]; and L is the Pt loading in the electrode (g/cm^2).

A comparison of the voltammetry of Pt/SiC and Pt/C in Fig. 5 also shows the difference in the onset potential for the oxide formation on Pt (accepted as Pt-OH) at around +0.8 V vs RHE. In the case of Pt/SiC, the shift of onset potential for the oxide formation is about +50 mV compared to the Pt/C catalyst. It clearly indicates the strong metal-support interactions between Pt and SiC compared to the Pt and carbon. As a result of strong interactions, there will be significant changes in the electronic states of surface platinum in such a way it inhibited the formation of -OH species, which will be a poisoning species for oxygen reduction. This may be beneficial to the oxygen adsorption at low overpotential and thus the ORR kinetic enhancement [25-28].

Fig. 6 shows the linear sweep voltammograms (LSVs) of Pt/SiC and commercial Pt/C catalysts between +0.2 and +1.2 V vs NHE at a scan rate of 2 mV/sec. From the figure, the ORR on all the catalysts is diffusion-controlled when the potential is less than +0.7 V and is under mixed diffusion-kinetic control in the potential region between +0.7 and +0.9 V vs NHE [29]. For both the Pt/SiC and Pt/C catalysts, when the potential was swept from +1.2 to +0.2 V, single oxygen reduction peak is observed in the potential region of ca. 1.0–0.7 V. Moreover, the steep increase in peak current at +0.7 V indicates the facile kinetics of ORR. Similar onset potential for oxygen reduction (+910 mV vs NHE) and shape of LSVs indicates that the ORR pathway and rate-determining step are the same on both Pt/SiC and Pt/C catalysts [30]. Oxygen reduction activity of the as-synthesized Pt/SiC is calculated to be 1.3 mA cm^{-2} where as for commercial 20% Pt/C (E-TEK) electrode it is 1.5 mA cm^{-2}. Since the amount of Pt loaded on SiC and carbon supports was not same, the better way to compare them is the mass activity. Mass activities are calculated by dividing the specific activity (mA/cm^2) by amount of Pt loading ($\mu g/cm^2$). The calculated mass activities (A/g) are shown in Table 1. The mass activity of Pt/SiC (18.4 wt% Pt) is 26 A/g whereas in the case of commercial Pt/C (19.7 wt% Pt) it is 27.6 A/g. It indicates that the oxygen reduction activity of the as-synthesized Pt/SiC is comparable to that of the commercial Pt/C (E-TEK) catalyst.

The current density–time plots of Pt/SiC and commercial Pt/C (E-TEK) in oxygen saturated 0.5 M H_2SO_4 at +0.7 V vs NHE are shown in Fig. 7. After 170 min, the activity of Pt/SiC is almost similar to that of Pt/C under the similar experimental conditions. In the case of commercial Pt/C catalyst, the current density decreases rapidly where as in the

case of as-synthesized Pt/SiC catalyst, the current density is not much degraded. The degradation of 25% and 35% of initial activity is observed for the Pt/SiC and Pt/C respectively. The low degradation of activity of Pt/SiC is due to the embedded Pt nanoparticles in the SiC support matrix by means of synthesis conditions and strong metal-support interactions. This is in good agreement with that of TEM analysis (inset of Fig. 3(b)) which reveals the embedded Pt particles in SiC matrix and cyclic voltammetric behaviour (Fig. 5) which shows the inhibition of -OH poisoning species and lower amounts of –OH formation on Pt supported SiC.

4. Summary

Ultrafine SiC was synthesized by thermal plasma method and used as support of Pt. Hydrogen reduction method was employed for the preparation of Pt/SiC. These materials were characterized by XRD, SEM, EDX and TEM. The oxygen reduction activity measurements performed on Pt/SiC indicate that the ORR activity of the Pt/SiC is comparable to that of the commercial Pt/C (E-TEK) catalyst. Current density-time plots reveal the lower degradation of activity of Pt/SiC compared to that of the commercial Pt/C catalyst.

5. References

1. B. Viswanathan and M. Aulice Scibioh (Eds.), *Fuel cells – Principles and Applications*; Universities Press (India) Private Limited, **2006**.
2. K. Kinoshita, *Carbon: Electrochemical and Physicochemical Properties*, Wiley, New York (1988).
3. D. A. Stevens and J. R. Dahn, *Carbon* 43 (2005) 179.
4. N. Giordano, P. L. Antonucci, E. Passalacqua, L. Pino, A. S. Arico and K. Kinoshita, *Electrochim. Acta* 36 (1991) 1931.
5. P. Stonehart,. *Progress in Batteries & Solar Cells* 5 (1984) 260.
6. T. R. Ralph and M. P. Hogarth, *Platinum Met. Rev.* 46 (2002) 3.

7. L. M. Roen, C. H. Paik and T. D. Jarvic, *Electrochemical and Solid-State Letters*, 7 (2004) A19.
8. J. Willsau and J. Heitbaum, *J. Electroanal. Chem.* 161 (1984) 93.
9. E. Passalacqua, P. L. Antonucci, M. Vivaldi, A. Patti, V. Antonucci, N. Giordano and K. Kinoshita, *Electrochim. Acta* 37 (1992) 2725.
10. V. Jalan, E. T. Taylor, D. Frost and B. Morriseau, National Fuel Cell Seminar Abstracts, Orlando, FL, Nov. 13-16, 1983, Courtesy Associates, Inc., Washington, DC (1983) p. 127.
11. A. Honji, T. Marl, and Y. Hishinuma, K. Kurita, *J. Electrochem. Soc.* 135 (1988) 917.
12. M. B. Kizling and S. G. Jaras, *Applied Catalysis A: General* 147 (1996) 1.
13. S. K. Singh and A. K. Sahoo, *Indian Patent* 393/DEL/2006.
14. M. A. Vannice, Yu-Lin Chao and R. M. Friedman, *Applied Catalysis,* 20 (1986) 91.
15. M. Balcerzak, E. Swiecicka and E. Balukiewicz, *Talanta* 48 (1999) 39.
16. T. J. Schmidt, H. A. Gasteiger, G. D. Stab, P. M. Urban, D. M. Kolb and R. J. Behm, *J. Electrochem. Soc.* 145 (1998) 2354.
17. F. Su, X. S. Zhao, Y. Wang, J. Zeng, Z. Zhou and J. Y. Lee, *J. Phys. Chem*. B 109 (2005) 20200.
18. U. A. Paulus, T. J. Schmidt, H. A. Gasteiger and R. J. Behm, *J. Electroanal. Chem.* 495 (2001) 134.
19. G. Tamizhmani, J. P. Dodelet and D. Guay, *J. Electrochem. Soc.* 143 (1996) 18.
20. C. L. Liang and A. L. Juliard, *J. Electroanal. Chem.* 9 (1965) 390-394.
21. N. M. Markovic, H. A. Gasteiger and P. N. Ross, *J. Electrochem. Soc.* 144 (1997) 1591.
22. A. Panchenko, M. T. M. Koper, T. E. Shubina, S. J. Mitchell and E. Roduner, *J. Electrochem. Soc.* 151 (2004) A2016.
23. A. Pozio, M. De Francesco, A. Cemmi, F. Cardellini and L. Giorgi, *J. Power Sources* 105 (2002) 13.
24. J. O'M Bockris, B.E. Conway (Eds.), Modern Aspects of Electrochemistry, vol. 12, Plenum Press, New York, 1977.
25. S. Mukerjee, S. Srinivasan, M. P. Soriaga and J. McBreen, *J. Electrochem. Soc.* 142 (1995) 1409.

26. V. Stamenkovic, T. J. Schmidt, P. N. Ross and N. M. Markovic, *J. Phys. Chem.* B 106 (2002) 11970.

27. V. Stamenkovic, T. J. Schmidt, P. N. Ross and N. M. Markovic, *J. Electroanal. Chem.* 554-555 (2003) 191.

28. A. Anderson, *Electrochim. Acta* 47 (2002) 3759.

29. H. Yang, W. Vogel, C. Lamy, and N. Alonso-Vante, *J. Phys. Chem.* B 108 (2004) 11024.

30. Q. Huang, H. Yang, Y. Tang, T. Lu and D. L. Akins, *Electrochem. Commun.* 8 (2006) 1220.

Figure captions

Fig. 1. Powder X-ray diffraction patterns of (a) SiC (b) Pt/SiC and (c) commercial Pt/C (E-TEK)

Fig. 2. SEM images of (a) SiC and (b) Pt/SiC

Fig. 3. TEM images of (a) SiC (b) Pt/SiC (inset shows the high magnification image) and (c) commercial Pt/C (E-TEK)

Fig. 4. EDX spectra of (a) SiC and (b) Pt/SiC

Fig. 5. Cyclic voltammograms (CVs) of (■) Pt/SiC and (●) commercial Pt/C (E-TEK) catalysts in Ar-saturated 0.5 H_2SO_4; Scan rate – 25 mV sec^{-1}

Fig. 6. Linear sweep voltammograms (LSVs) of O_2 reduction on (■) Pt/SiC and (●) commercial Pt/C (E-TEK) catalysts in 0.5 H_2SO_4; Scan rate – 2 mV sec^{-1} (Empty symbols corresponding to the LSVs in Ar-saturated 0.5 M H_2SO_4)

Fig. 7. Current density - time plots of (■) as-synthesized Pt/CDX975 and (●) commercial Pt/C (E-TEK) measured in oxygen saturated 0.5 M H_2SO_4 at +0.7 V vs NHE

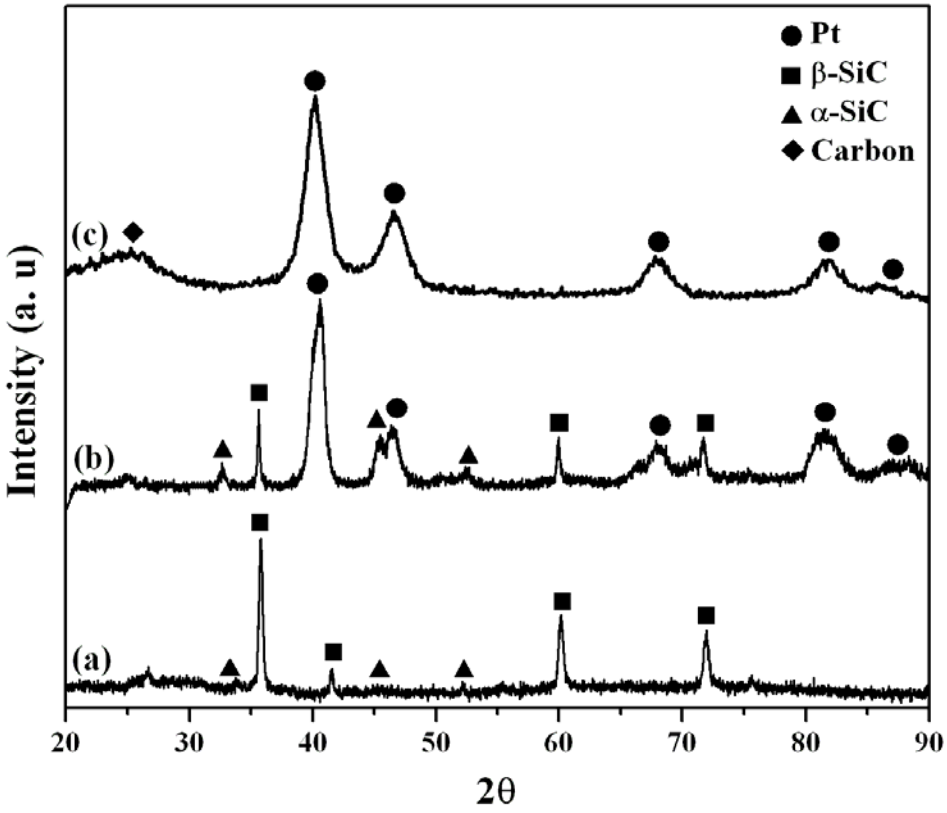

Fig. 1

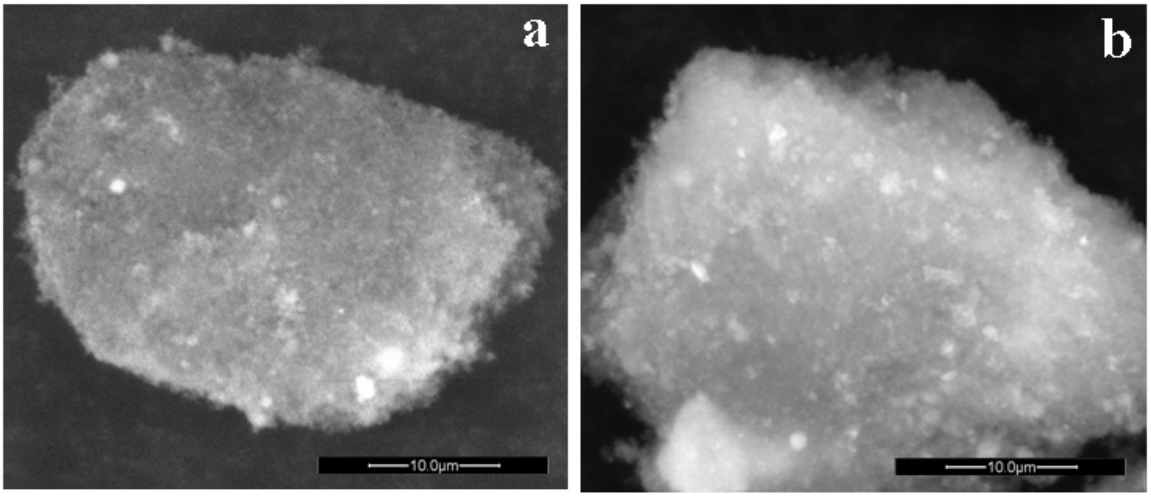

Fig. 2

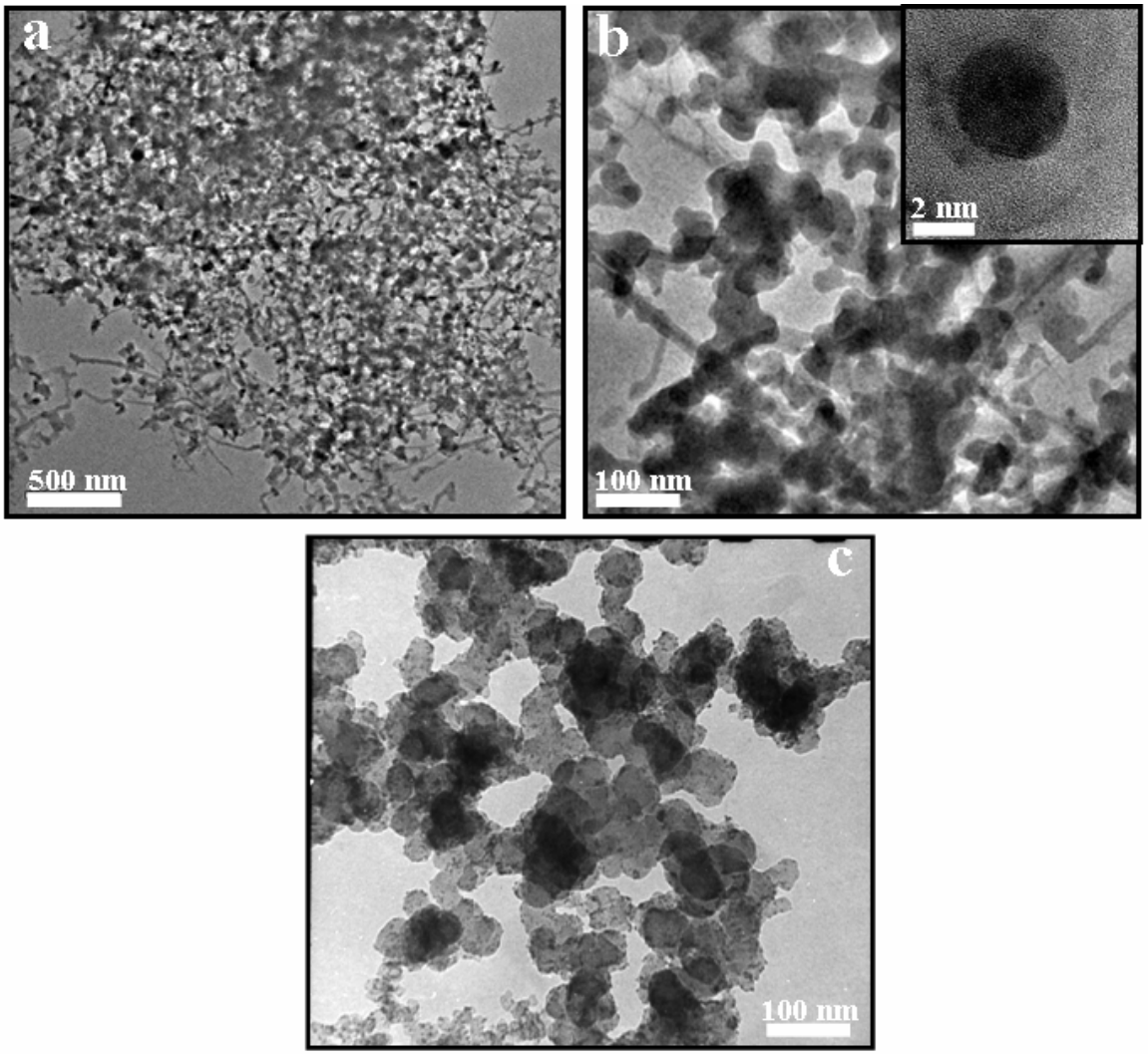

Fig. 3

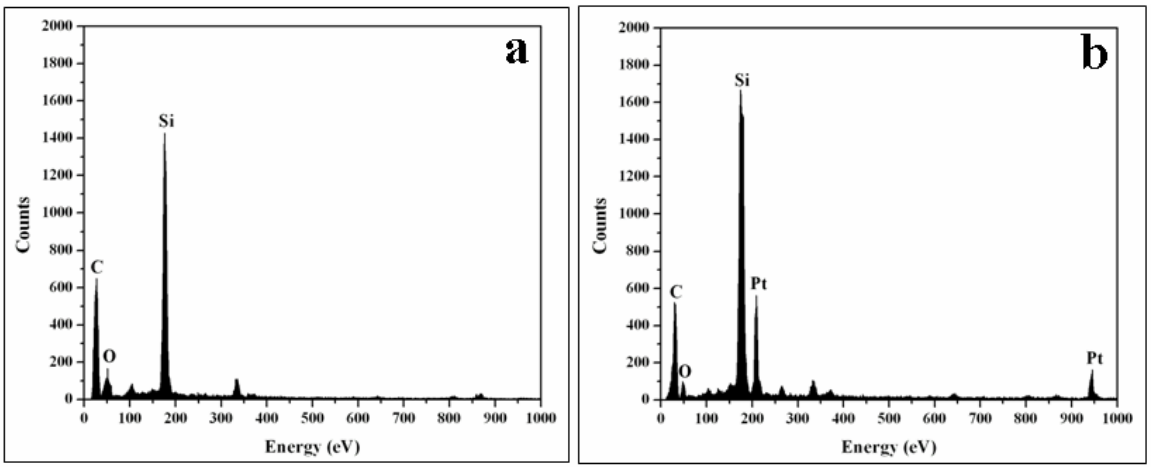

Fig. 4

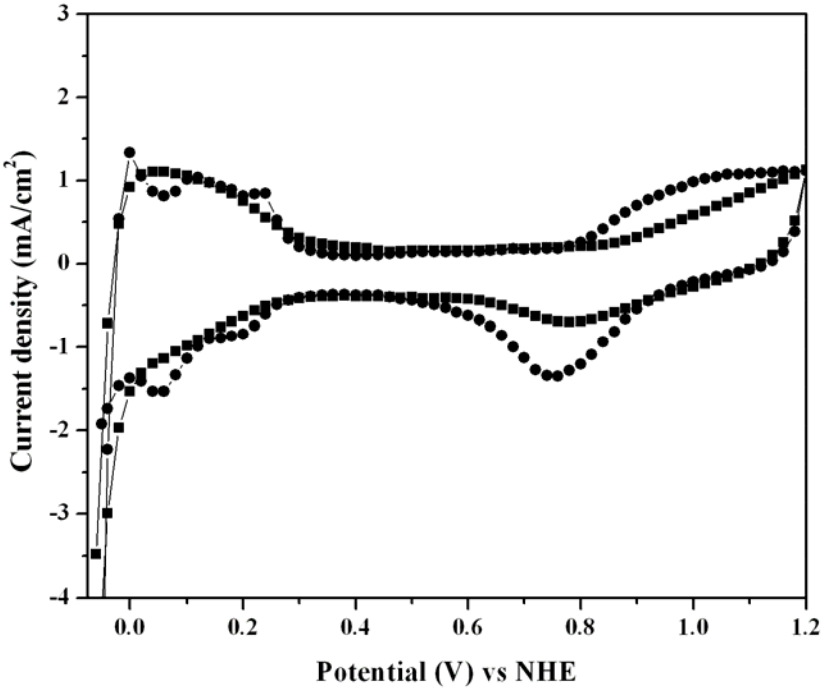
Current density (mA/cm^2)
Potential (V) vs NHE
3
2
1
0
-1
-2
-3
-4
0.0
0.2
0.4
0.6
0.8
1.0
1.2

Fig. 5

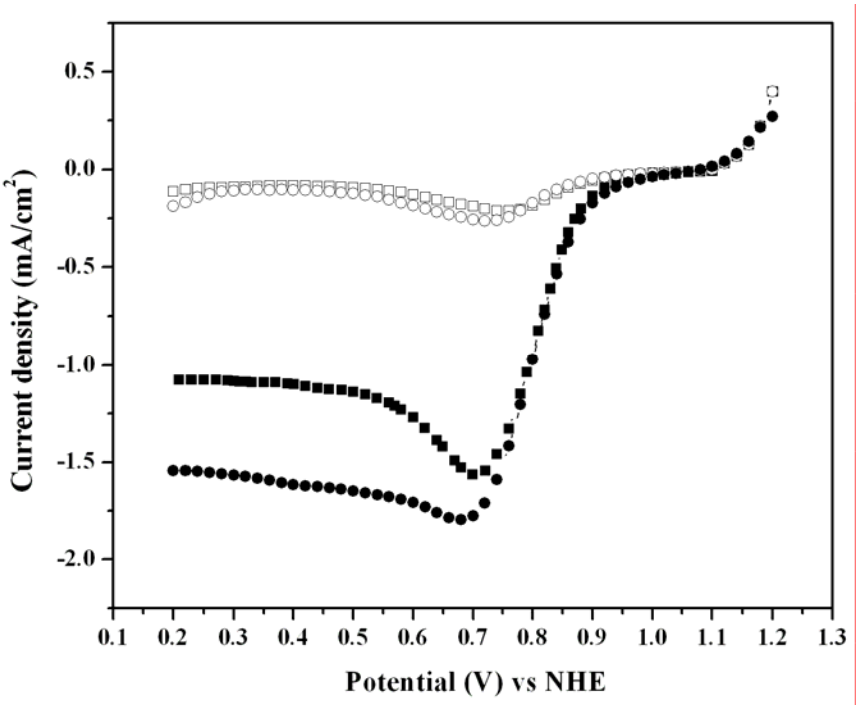
Current density (mA/cm^2)
0.5
0.0
-0.5
-1.0
-1.5
-2.0
0.1
0.2
0.3
0.4
0.5
0.6
0.7
0.8
0.9
1.0
1.1
1.2
1.3
Potential (V) vs NHE

Fig. 6

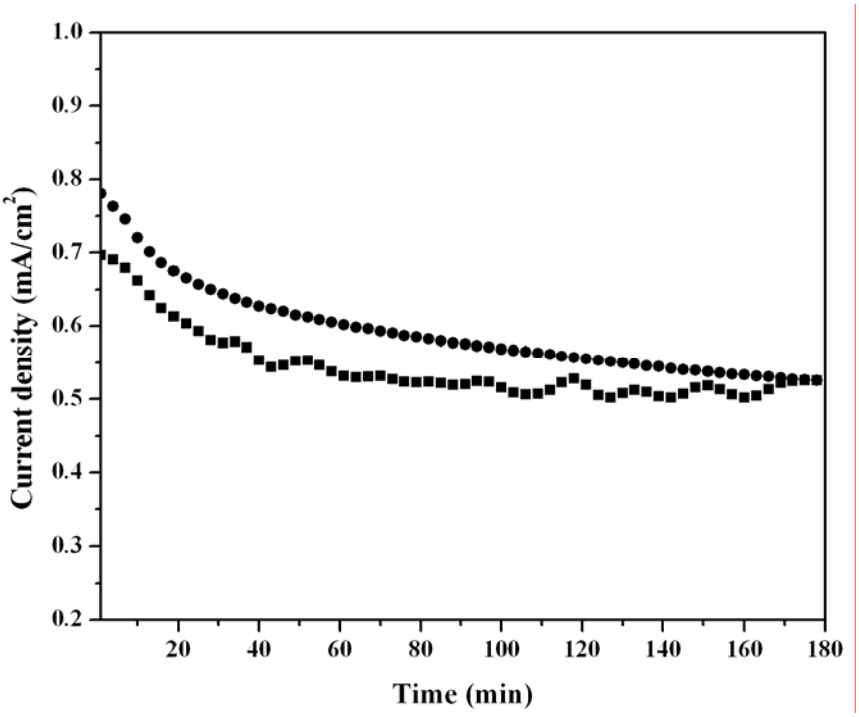
Current density (mA/cm^2)
1.0
0.9
0.8
0.7
0.6
0.5
0.4
0.3
0.2
20
40
60
80
100
120
140
160
180
Time (min)

Fig. 7

Table 1. Estimated Pt loading, Pt particle size, specific surface area and oxygen reduction activities of as-synthesized Pt/SiC and commercial Pt/C catalysts

Catalyst	Pt loading[a] (wt.%)	Pt particle size[b] (nm)	Specific surface area of Pt[b] (m^2/g)	Electroactive Surface area[c] (m^2/g)	ORR activity at +0.7 V vs NHE (A/g)
As-synthesized Pt/SiC	18.4	3.5±0.6	76±15	73±10	26
Commercial Pt/C (E-TEK)	19.7	3.7±0.2	81±10	80±10	27.2

[a]from spectrophotometric measurements; [b]from TEM measurements;
[c]from cyclic voltammetry measurements